 CMES, vol.53, no.2, pp.181-206, 2009

Computation of the Turbulent Flow in a Square Duct Using a Cubic Low-Reynolds Stress Model

H. Naj [1, 2, 3] **and G. Mompean**[1,2]

Abstract: The aim of this work is to predict numerically the turbulent flow through a straight square duct using a nonlinear stress-strain model. The paper considers the application of the Craft et al.'s model [Craft, Launder, and Suga (1996)] to the case of turbulent incompressible flow in a straight square duct. In order to handle wall proximity effects, damping functions are introduced. Using a priori and a posteriori investigations, we show the performance of this model to predict such flows. The analysis of the flow anisotropy is made using the anisotropy-invariant map proposed by Lumley and Newman [Lumley and Newman (1977)]. This map shows the various possible states of the turbulence. The mean flow field and the turbulent statistics are compared with existing numerical and experimental data for square and rectangular duct flows. Overall, the model performance is shown to be satisfactory. In particular, the mean secondary velocity field and the streamwise vorticity are well predicted.

Keywords: Computational fluid mechanics; Finite volume method; cubic $k-\varepsilon$ model; realizability; square duct flow.

1 Introduction

The turbulence flow inside a duct of square cross-section is of considerable engineering interest, with relevance to flow in the root region of a lifting section, complex flow in turbomachinery and heat exchangers, flows in ducts with non-circular cross-section, and flows in open channels and rivers. This flow is characterized by the existence of secondary flows which can be classified into two types, namely, Prandtl's flows of the first and second kind. In general, numerical predictions of turbulent flows have become a valuable tool to obtain a detailed description of the turbulent flows which are difficult to obtain experimentally.

[1] Université Lille 1 - Sciences et Technologies, LML UMR CNRS 8107, Boulevard P. Langevin, F-59655 Villeneuve d'Ascq, France.
[2] LML UMR CNRS 8107, Boulevard P. Langevin, F-59655 Villeneuve d'Ascq, France.
[3] Corresponding author, hassan.naji@polytech-lille.fr

In the past years, several formulations have been developed in order to solve CFD problems for laminar and turbulent flow, using mesh and meshfree methods. The Eulerian formulation where the mesh is fixed in space is commonly used to solve incompressible fluid problems for academic and industrial applications. These formulations can be based on implicit velocity pressure coupling procedure using finite element or finite volume analysis as described in Longatte et al. (2003), or velocity pressure decoupling procedure using staggered-mesh finite volume method. This method is used in Aquelet et al. (2003) to solve free surface flow and sloshing tank problems. Some recent works in engineering applications used meshless methods. These methods are used for fluid dynamics as well as for structure dynamics as described in Lin and Atluri (2001), Ahrem et al. (2006), Arefmanesh et al. (2008), and Zheng at al. (2009). These methods are developed for explicit time integration algorithms and are mainly used to solve compressible, nearly incompressible, and incompressible flows, as described in Vertnik and Šarler (2009), Pasquim and Mariani (2008), and Orsini et al. (2008).

Attempts to predict the turbulent characteristics have resulted in several computational approaches which can generally be classified as DNS (Direct Numerical Simulation), LES (Large Eddy Simulation) or RANS (Reynolds Averaged Navier-Stokes). The DNS approach is a simulation in computational fluid dynamics in which the Navier-Stokes equations are solved numerically without any turbulence modelling. This means that the whole range of spatial and temporal scales of the turbulence must be resolved. All the spatial scales of the turbulence must be resolved in the computational mesh, from the smallest dissipative scales (Kolmogorov microscales) up to the integral scale L, associated with the motions containing most of the kinetic energy. The results from the DNS are accurate and reveal valuable information on the turbulence structures. In 1992, Gavrilakis [Gavrilakis (1992)] reported on DNS of square duct flow. These simulations, providing mean-flow properties and turbulent statistics, have been used to estimate each term in the mean streamwise vorticity equation. Huser and Birigen [Huser and Birigen (1993)] simulated square duct flow using DNS and demonstrated that the mean secondary flows are related to the ejection structures near the wall. However, two of the major shortcomings of the DNS simulations are their exertion only at low or moderate Reynolds numbers, because the number of grid points increases as $Re^{9/4}$ where Re is the Reynolds numbers, and the computational demands are very large (requiring hundreds of hours of CPU time on the super computers). Therefore, the DNS approach is limited to low Reynolds numbers. An alternative to the DNS approach is the technique of LES. The LES approach is a numerical technique used to solve the partial differential equations governing turbulent fluid flow. It was formulated in the late 1960s and became popular in the later years. It was first used by Joseph

Smagorinsky to simulate atmospheric air currents, so its primary use at that time was for meteorological calculations and predictions. In 1991, Madabhushi and Vanka [Madabhushi and Vanka (1991)] were the first investigators to the perform LES of the square duct flow. However, the LES approach requires less computational effort than DNS but more effort than those methods that solve the Reynolds-averaged Navier-Stokes equations (RANS). The RANS approach required for the derivation of the RANS equations from the instantaneous Navier–Stokes equations is the Reynolds decomposition. Reynolds decomposition refers to separation of the flow variable into the mean component and the fluctuating component. However, when using this approach, the success of computational results depends heavily on the choice of the Reynolds Stress Model (RSM). In the RSM model, which is proposed initially by Launder et al. [Launder, Reece, and Rodi (1975)], the pressure-strain correlation terms incorporate the non-local effect of the flow. The RSM is extremely complicated to solve for complex three-dimensional flows, the modelled terms require a variety of ad hoc wall damping functions and the numerical values of the coefficients are chosen based on empiricism [Gibson and Launder (1978); Speziale, Sarkar, and Gatski, (1991)]. In order to combine simplicity, generality and efficiency, explicit algebraic Reynolds stress models (EARSM) have been proposed in the literature. These EARSM models propose the relations between Reynolds stress tensor, mean rate of deformation and the vorticity tensors, and they are able to capture more characteristics of the turbulent flows (anisotropy, near-wall behaviour). Historically speaking, Rodi [Rodi (1976)] was the first to derive a two-equation algebraic Reynolds stress model. This methodology has since further advanced by Taulbee [Taulbee (1992)], Speziale [Speziale (1987)], Gatski and Speziale [Gatski and Speziale (1993)] and Jongen et al. [Jongen, Mompean, and Gatski (1998)]. There are two different strategies to derive EARSM models. The first one uses the equilibrium second moment equation with a partial constitutive relation. In this category, we can find several models. Among these, we can cite those proposed by Taulbee [Taulbee (1992)], Wallin and Johansson [Wallin and Johansson (2000)] and Gatski and Rumsey [Gatski and Rumsey (2001)]. The second alternative uses general constitutive relations for the Reynolds stress manipulated with the invariance and the realizability, Pope [Pope (1975)], the rapid distortion theory and the renormalization group analysis. We can cite, in this second strategy, the models developed by Yoshizawa [Yoshizawa (1984)], Rubinstein and Barton [Rubinstein and Barton (1990)], Shih and Lumley [Shih and Lumley (1995)], Craft et al. [Craft, Launder, and Suga (1996); Craft, Lacovides, and Yoon (1999)].

This work focuses on a numerical investigation of a low Reynolds number turbulent flow though a square duct with emphasis on EARSMs model, which are based on the general constitutive equations and which have been derived by Craft et al.

[Craft, Launder, and Suga (1996); Craft, Lacovides, and Yoon (1999)]. These models have been proposed to extend the applicability of many quadratic models, Shih et al. [Shih, Zhu, and Lumley (1995)]. Note that, the Craft et al.'s model is a cubic relation between the strain and vorticity tensor and the stress tensor, and according these authors, it seems more appropriate to reflect the effects of curvature and swirling. Therefore, the present study aims at investigating the capability of this cubic viscosity turbulence model in the fully turbulence flow through a straight square duct. This square duct configuration has been frequently chosen by many authors (Gavrilakis [Gavrilakis (1992)], Madabhushi and Vanka [Madabhushi and Vanka (1991)], Huser and Biringen [Huser and Biringen (1993)], Mompean et al. [Mompean, Gavrilakis, Machiels, and Deville (1996)], Xu and Pollard [Xu and Pollard (2001)], Xu et al. (2003) [Xu, Khalid, and Pollard (2003)], etc...) since it is a relatively simple geometry which provides a good test case to improve turbulence models performance. Note that this flow is strongly anisotropic and involves a secondary flow in the cross-stream plane, which is absent in the case of a plane channel.

The paper is organised as follows: The EARSM model herein employed is briefly described in the second section. The third section contains a brief outline of the finite volume numerical method. The main results of this work are presented and discussed in the fourth section, followed by conclusions drawn from the present predictions.

2 Governing equations

In the present work, RANS formulation is used to predict the turbulent flow. This approach is used applying the Reynolds decomposition, which consists of splitting the velocity and pressure variables into an average and a fluctuating part. The equations governing the mean velocity U_i and the mean pressure P are obtained from the RANS equations for incompressible flow:

$$\begin{aligned} &\frac{\partial U_i}{\partial x_i} = 0 \\ &\frac{\partial U_i}{\partial t} + \frac{\partial}{\partial x_j}\left(U_i U_j\right) - \frac{\partial}{\partial x_j}\left(\nu \frac{\partial U_i}{\partial x_j} - \overline{u_i' u_j'}\right) + \frac{1}{\rho}\frac{\partial P}{\partial x_i} = 0 \end{aligned} \tag{1}$$

where is the fluid density, is the cinematic viscosity and $\overline{u_i' u_j'}$ is the Reynolds stress tensor. The indices refer to the x, y, and z directions, respectively; x is the streamwise and y and z are the transverse directions.

To close the RANS equations (1), the cubic eddy-viscosity model of turbulence proposed by Craft et al. [Craft, Launder, and Suga (1996); Craft, Lacovides, and

Yoon (1999)] is used. The most general expression retaining terms up to cubic level that satisfies the required symmetry and contraction properties, can be written as follows:

$$\begin{aligned}\overline{u_i'u_j'} =& \frac{2}{3}k\delta_{ij} - \nu_t S_{ij} + c_1\frac{\nu_t k}{\tilde{\varepsilon}}(S_{ik}S_{jk} - 1/3S_{kl}S_{kl}\delta_{ij}) \\ &+ c_2\frac{\nu_t k}{\tilde{\varepsilon}}(\Omega_{ik}S_{jk} + \Omega_{jk}S_{ik}) + c_3\frac{\nu_t k}{\tilde{\varepsilon}}(\Omega_{ik}\Omega_{jk} - 1/3\Omega_{kl}\Omega_{kl}\delta_{ij}) \\ &\longleftarrow \text{quadrati terms} \longrightarrow \\ &+ c_4\frac{\nu_t k^2}{\tilde{\varepsilon}^2}(S_{ki}\Omega_{lj} + S_{kj}\Omega_{li})S_{kj} \\ &+ c_5\frac{\nu_t k^2}{\tilde{\varepsilon}^2}(\Omega_{il}\Omega_{lm}S_{mj} + S_{il}\Omega_{lm}\Omega_{mj} - 2/3S_{lm}\Omega_{mn}\Omega_{nl}\delta_{ij}) \\ &+ c_6\frac{\nu_t k^2}{\tilde{\varepsilon}^2}S_{ij}S_{kl}S_{kl} + c_7\frac{\nu_t k^2}{\tilde{\varepsilon}^2}S_{ij}\Omega_{kl}\Omega_{kl} \\ &\longleftarrow \text{cubic terms} \longrightarrow\end{aligned} \tag{2}$$

where $k(=\overline{u_j'u_j'}/2)$ is the turbulent kinetic energy, $\nu_t(=C_\mu k^2/\tilde{\varepsilon})$ is the turbulent viscosity, $\tilde{\varepsilon}(=\varepsilon - 2\nu(\partial k^{1/2}/\partial x_j)^2)$ is the "isotropic" dissipation rate, δ_{ij} is the Kronecker tensor, and S_{ij} and Ω_{ij} are the mean rate of deformation and vorticity tensors, respectively.

The model coefficients c_1, c_2, c_3, c_4, c_5, c_6 and c_7 in equation (2) are given in Table 1, where the coefficient C_μ is a function of the strain and vorticity invariants $\tilde{S}$ and $\tilde{\Omega}$:

$$C_\mu = \frac{0.3}{1+0.35\max(\tilde{S},\,\tilde{\Omega})^{3/2}}\left(1-\exp\left(-0.36\exp\left(0.75\max(\tilde{S},\,\tilde{\Omega})\right)\right)\right) \tag{3}$$

The nondimensional strain rate $\tilde{S}$ and vorticity $\tilde{\Omega}$ are denoted by $\tilde{S} = k/\tilde{\varepsilon}\sqrt{S_{ij}S_{ij}/2}$ and $\tilde{\Omega} = k/\tilde{\varepsilon}\sqrt{\Omega_{ij}\Omega_{ij}/2}$, respectively.

Table 1: The proposed form for the coefficients of equation 2.

C_1	C_2	C_3	C_4	C_5	C_6	C_7
-0.1	0.1	0.26	$-10C_\mu^2$	0.	$-5C_\mu^2$	$5C_\mu^2$

The cubic stress-strain relation (2) adopted here presents some advantages. Indeed, the quadratic terms and strain/vorticity-dependent coefficients are responsible for the ability of the non-linear models to capture flow anisotropy, and the cubic terms can reflect the effect of curvature. Also, theses cubic terms can capture the

swirling flow effect according to Pettersson and Andersson [Pettersson and Andersson (2002)].

The turbulence energy k and the "isotropic" dissipation rate $\tilde{\varepsilon}$ are obtained from the following transport equations:

$$\frac{Dk}{Dt} = P_k - \varepsilon + \frac{\partial}{\partial x_j}\left[\left(\nu + \frac{\nu_t}{\sigma_k}\right)\frac{\partial k}{\partial x_j}\right] \tag{4}$$

$$\frac{D\tilde{\varepsilon}}{Dt} = c_{\varepsilon 1}\frac{\tilde{\varepsilon}}{k}P_k - c_{\varepsilon 2}\frac{\tilde{\varepsilon}^2}{k} + E + Y_{ap} + \frac{\partial}{\partial x_j}\left[\left(\nu + \frac{\nu_t}{\sigma_\varepsilon}\right)\frac{\partial \tilde{\varepsilon}}{\partial x_j}\right]$$

where $\frac{D(.)}{Dt} = \frac{\partial(.)}{\partial t} + \overline{U}_j\frac{\partial(.)}{\partial x_j}$ is the total derivative, $P_k = \overline{u_i u_j}\frac{\partial U_i}{\partial x_j}$ is the turbulent energy production. The near-wall source term E, which in the Launder-Sharma model [Launder and Sharma (1974)], takes the form of $2\nu\nu_t(\partial^2\overline{U}_i/\partial x_j\partial x_k)^2$, is modified to reduce its dependence on the Reynolds number. Consequently, it is modelled as follows:

$$\begin{cases} E = 0.0022\frac{\tilde{S}\nu_t k^2}{\tilde{\varepsilon}}\left(\frac{\partial^2\overline{U}_i}{\partial x_j\partial x_k}\right)^2 & \text{if } Re_t \le 250 \\ E = 0 & \text{if } Re_t > 250 \end{cases} \tag{5}$$

The length-scale correction Y_{ap} proposed by Yap [Yap (1987)] can be expressed as follows:

$$Y_{ap} = 0.83\frac{\tilde{\varepsilon}^2}{k}\max\left(\left[\frac{k^{1.5}}{2.5\tilde{\varepsilon}y} - 1\right]\left[\frac{k^{1.5}}{2.5\tilde{\varepsilon}y}\right]^2, 0\right) \tag{6}$$

The various coefficients are given in Table 2.

Table 2: Coefficients in and equations

$C_{\varepsilon 1}$	$C_{\varepsilon 2}$	σ_k	σ_ε
1.44	$1.92(1-0.3\exp(-R_t^2))$	1.0	1.3

3 Direct simulation

3.1 Direct Numerical simulation

In this paper, we used the Gavrilakis data [Gavrilakis (1992)] for a priori tests. For this simulation, the flow variables are expanded into discrete Fourier series along the x-direction, whereas second-order centred-difference approximations are

used along y and z-directions. The Adams-Bashforth scheme is used for the temporal integration. This DNS has been carried out for the Reynolds number $Re = \overline{U}_m 2h/\nu = 4410$ based on the duct height 2h and the mean flow velocity $\overline{U}_m$. The Reynolds number $Re^+ = u_\tau 2h/\nu$ based on the shear velocity is 300. The velocity ratio $\overline{U}_0/\overline{U}_m$ for this configuration was 1.33, $\overline{U}_0$ being the mean centreline velocity. The maximum Kolmogorov scale is $1.5\nu/u_\tau$. For more details on DNS, we can refer to the paper of Gavrilakis [Gavrilakis (1992)].

3.2 Direct evaluation of the Craft et al. cubic model

3.2.1 Numerical methodology and damping functions

The a priori technique consists in using turbulent mean field predicted by DNS. The mean velocity components, the turbulent kinetic energy and its dissipation rate obtained through the DNS simulations are used in the turbulent model, to predict the Reynolds stresses. The predictions are then compared with these quantities obtained directly from the DNS. Figure 1 illustrates this a priori test.

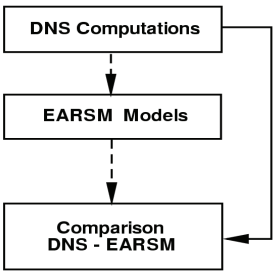

Figure 1: Schematic diagram showing the structure of a priori test.

The geometrical configuration of the square duct with the reference axes is shown in Fig. 2(a). The x-axis designates the streamwise direction. The normal direction is parallel to the y-axis and the spanwise direction is parallel to the z-axis. The cross-section is divided into four quadrants. Because of symmetry, only quadrant of the square duct need to be calculated with symmetry conditions at the wall bisectors (cf. Fig. 2).

As the flow through the straight square duct is supposed periodic in the streamwise direction, a two-dimensional mesh is sufficient for this study. Therefore, the calculations were carried out using 63×63 grid points, irregularly spaced in the

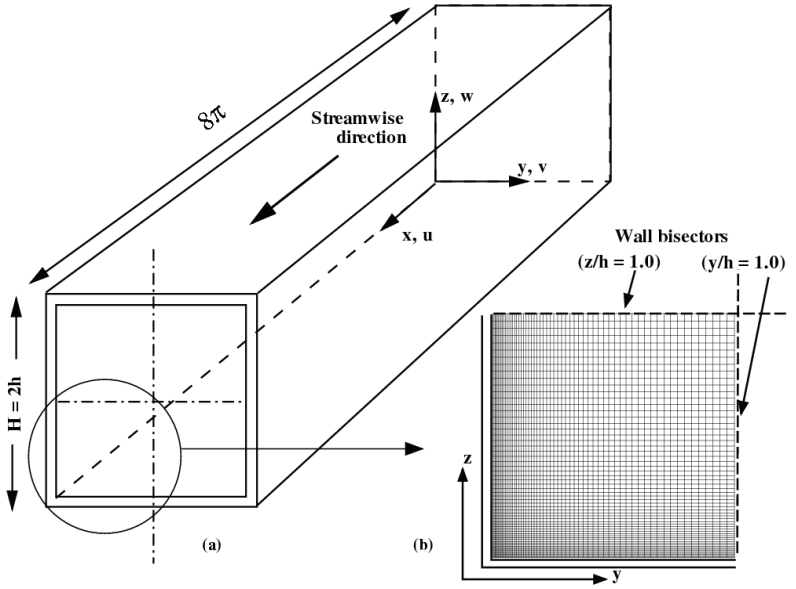

Figure 2: (a) Sketch of the computational domain; (b) Quadrant of the square.

cross-section (cf. Fig. 2(b)). The terms in the EARSM equation are discretized in space using the first Euler order upwind scheme.

To enable a correct behaviour in the regions close to the walls, damping functions of Van Driest types (Van Driest, 1956) have been used to bridge the solution. These functions are given by (see Naji et al. [Naji, Mompean, and El Yahyaoui (2004)]):

$$f = (1 - a\exp(-bz^+))(1 - a\exp(-by^+)) \tag{7}$$

where $z^+(= zu_\tau/\nu)$ and $y^+(= yu_\tau/\nu)$ are the nondimensional coordinates scaled by the kinematic viscosity ν and the mean frictional velocity , being the mean wall shear stress. The constants a and b (see Tab. 3) used here are those best corroborate the DNS of Gavrilakis through our various a priori tests. Throughout this paper, the modified model (see Eqs. (2)-(6) and (7)) will be labelled Craft$_f$ et al.

From Table 3, one can note that all the normaized Reynolds stresses $< u_i u_j >$ $(= \overline{u_i' u_j'}/u_\tau^2)$ have different damping functions.

Table 3: Values of constants $\boldsymbol{a}$ and $\boldsymbol{b}$ used in the damping function f_μ.

	$\langle u^2 \rangle$	$\langle v^2 \rangle$	$\langle w^2 \rangle$	$-\langle uv \rangle$	$\langle uw \rangle$	$\langle vw \rangle$
a	-4.5	0.34	0.34	1.01	1.01	0.68
b	0.038	0.05	0.05	0.04	0.04	0.043

3.2.2 Numerical results and discussion

To check if the Craft et al.'s model [Craft, Launder, and Suga (1996)] reproduces the anisotropic character of the flow, a detailed analysis of the flow anisotropy may be performed via the anisotropy-invariants map proposed by Lumley and Newmann [Lumley and Newmann (1977)]. They have identified all turbulence sates in terms of second () and third () invariants of the Reynolds stress anisotropy tensor b_{ij} which is defined as:

$$b_{ij} = (\overline{u_i u_j} - \tfrac{2}{3} k \delta_{ij})/2k \tag{8}$$

The second and third invariants are defined by:

$$II_b = -b_{ij} b_{ji}/2 \quad III_b = b_{ij} b_{jk} b_{ki}/3 \tag{9}$$

It can be shown that all the turbulence sates which characterize the turbulence are limited inside the region bounded by the axisymmetric and two-dimensional states.

Figure 3 shows the variation of against for the Reynolds stress along the wall bisector. The tendency of the turbulence sate is towards an axisymmetric state. However, the flow behaviour is affected by the corner and the turbulence tends to a one-dimensional state. Near the duct center, the turbulence is close to isotropy.

To verify the realizability of the current model (Craft et al.'s model), Figures 4, 5 and 6 present, respectively, the contours plots of the normal Reynolds stresses $< u^2 >$ and $< w^2 >$ and, the contours plots of the quantity $(< uw >^2)/(< u^2 >< w^2 >)$. Plotted are the DNS data by Gavrilakis [Gavrilakis (1992)] for comparison (see Figs. 4(b), 5(b) and 6(b)). Note that the distributions of $< v^2 >$ (resp. $(< uw >^2)/(< u^2 >< w^2 >)$) are similar to those of $< w^2 >$ (resp. $(< uv >^2)/(< u^2 >< v^2 >)$) so that $< w(y) >=< v(z) >$ *and* $< uw(y) >=< uv(z) >$. The contour plot of $< v^2 >$ (resp. $(< uv >^2)/(< u^2 >< v^2 >)$) is therefore obtained by 90° rotation of the $< w^2 >$ (resp. $(< uw >^2)/(< u^2 >< w^2 >)$) contour plot in the (y, z) plane. The distributions of these quantities in the other quadrant can be obtained through a symmetric mirroring with respect to the corresponding axes or origin. By the examination of these figures, we remark that the turbulent normal stresses are positive and the Schwarz inequality is respected $((< u_i u_j >^2)/(< u_i^2 >< u_j^2 >$

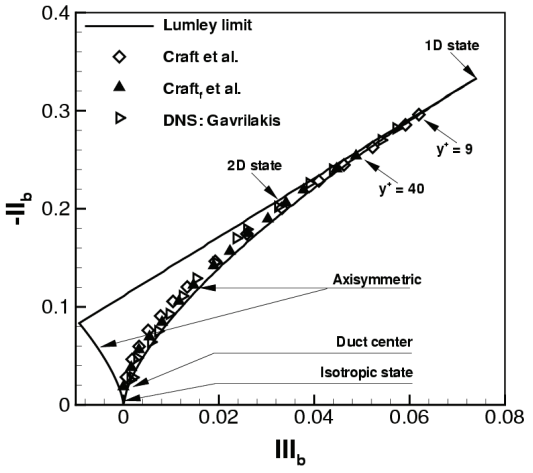

Figure 3: The trajectories in anisotropy map along the wall bisector.

$) \leq 1$). For all the Reynolds stresses, the comparison of the numerical results with available DNS shows good agreements.

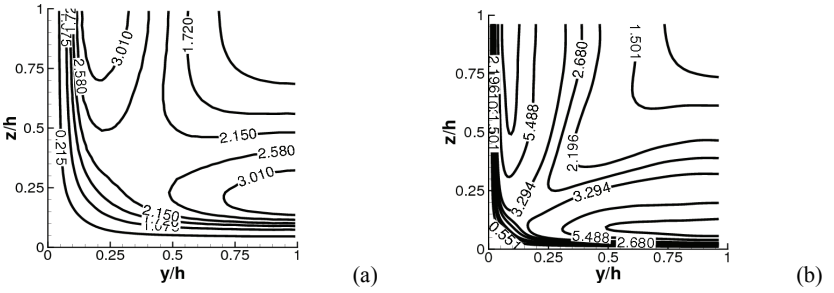

Figure 4: Contour plots of the normal Reynolds stresses $< u^2 >$: (a) present study; (b) DNS data from Gavrilakis (1992).

In Figure 7 (a, b and c), the normal profiles of the normalized turbulent stresses as functions of the z-direction along the wall bisector are represented and compared with DNS data obtained by Gavrilakis [Gavrilakis (1992)] and with the model results of Speziale [Speziale (1987)] and Gatski and Speziale [Gatski and Speziale (1993)]. As shown in Figure 7(a), the component $< u^2 >$ is best predicted by

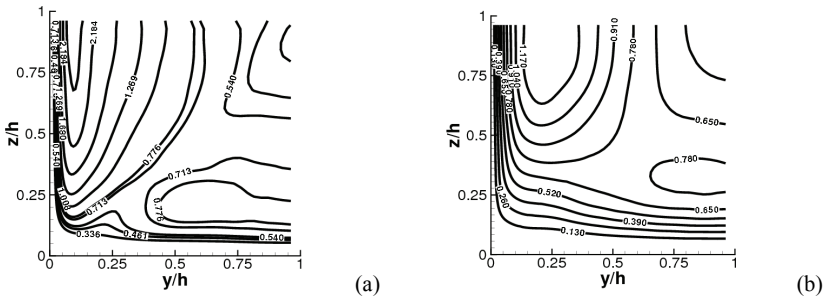

Figure 5: Contour plots of the normal Reynolds stresses$< w^2 >$: (a) present study; (b) DNS data from Gavrilakis (1992).

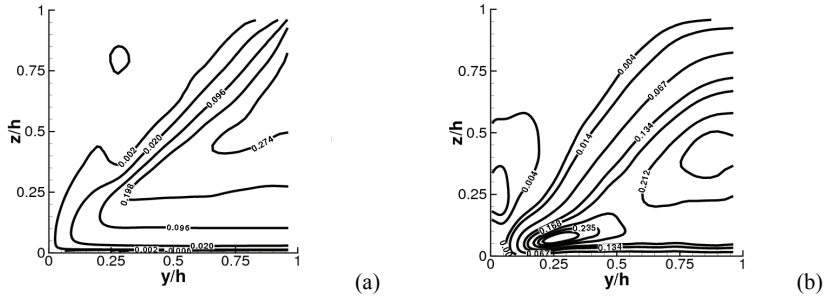

Figure 6: Contour plots of the quantities $< uw >^2 /(< u^2 >< w^2 >)$: (a) present study; (b) DNS data from Gavrilakis (1992).

the current EARSM model [Craft, Launder, and Suga (1996); Craft, Lacovides, and Yoon (1999)], although the peak is slightly underpredicted. The agreement here being satisfying, this suggest that the near wall turbulence generation mechanisms seem to be faithfully captured. One can observe that the $< u^2 >$ component dominates the other two components with a very marked peak close to the wall ($z/h \approx 0.1$).

For the y-component $< v^2 >$ (see Fig. 7(b)), the Craft$_f$ et al.'s model, while overpredicting the magnitude of this quantity compared with DNS results from Gavrilakis [Gavrilakis (1992)], duplicates the DNS far away from the wall for $z/h \geq 0.25$. Note that the peak is over-predicted by about 25% compared with the DNS and it is not reached at the same location as the DNS. Figure 7(b) clearly demonstrates that the spanwise turbulence component $< v^2 >$ is very sensitive to the choice of the model, in particular for $z/h \leq 0.25$.

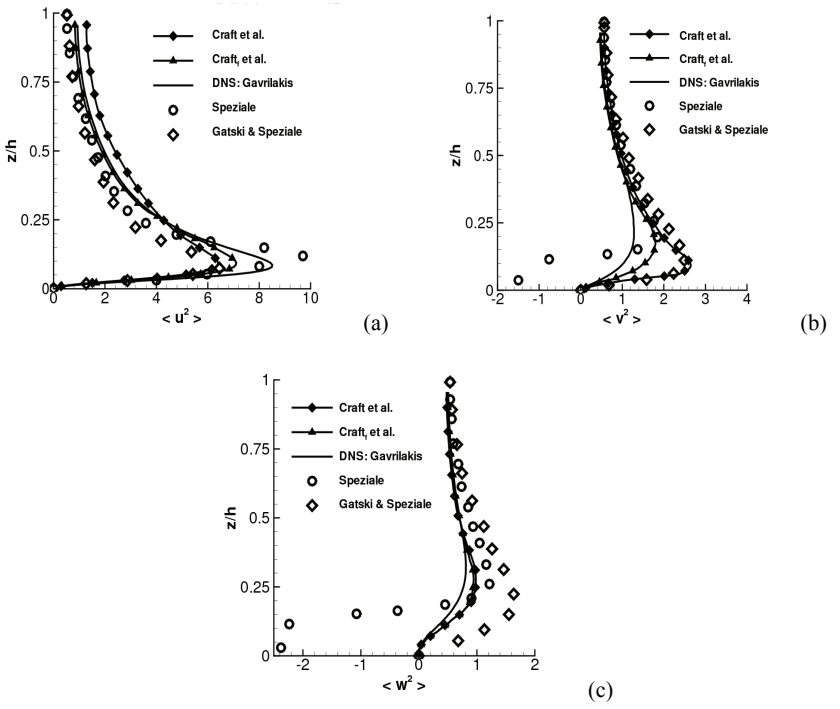

Figure 7: Normal profiles versus z/h. Comparison of Gavrilakis's DNS (1992) with the model estimates.

Also, it can be seen that its intensity increases rapidly in the near wall region, approximately corresponding to $0 \leq z/h \leq 0.1$ and that the predicted profiles are larger than the profile from the DNS. All models overpredict the magnitude of $< v^2 >$. The vertical turbulence component $< w^2 >$ (see Figure 7(c)), in the current model agrees well with the DNS data by Gavrilakis [Gavrilakis (1992)] for. However, our predictions tend to slightly overestimate this intensity in the near wall region. The peak value from the present model is predicted almost at the same location as the DNS.

Otherwise, some noticeable differences are found, by comparing our predictions with those of the Speziale [Speziale (1987)] and, Gatski and Speziale [Gatski and Speziale (1993)] models. As pointed out by several authors, the main difference among the profiles of the cross-stream turbulence intensities and that of the channel flow occurs in the zones close to the walls.

These discrepancies mainly affect the $< v^2 >$ component. These may be attributed

to the low Reynolds number used in this work and to the presence of the secondary flows in the cross-stream plane, that are absent in the case of a plane channel. Note that the Speziale model [Speziale (1987)] is not strongly realizable. Indeed, the spanwise and the vertical turbulence intensities are negative for $z/h \leq 0.20$ (see Figures 7(b) and 7(c)).

Figure 8 depicts the distribution of the Reynolds shear stress component $- < uv >$ and $- < uw >$ along the z-direction at the wall bisectory$/h = 1.0$. It can be seen that the shear stress component $- < uw >$ returned by the present model agrees well with the DNS for$^z/h \geq 0.25$. The $- < uw >$ peaks obtained by the two models (Craft et al. and Craft$_f$ et al.) are roughly the same and they are much higher than the corresponding peak of the DNS data.

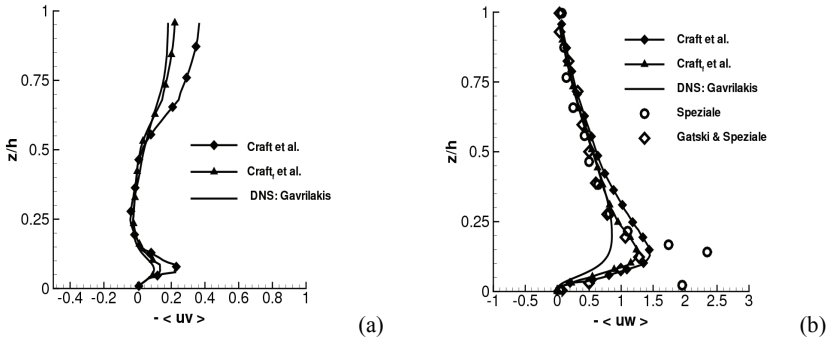

Figure 8: Shear stress profiles versus z/h. Comparison of Gavrilakis's DNS (1992) with the model estimates.

The a priori evaluation and improvement of Craft et al.'s model shows that it is able to predict turbulence flow through a straight square duct. Therefore, the extension to a posteriori evaluation of the turbulence flow should produce reliable predictions for other similar flows at a comparable Reynolds number.

4 A posteriori assessment of the Craft et al. cubic model

4.1 Spatial and temporal discretization

The governing equations are spatially discretized using a second-order finite volume method on a staggered grid. The conservation equations are integrated over a control volume of boundary, and the Gauss theorem is used to transform the volume integrals into surface integrals. The pressure, the turbulent kinetic energy, the "isotropic" dissipation rate and the normal Reynolds stress components are treated

in the centre of the control volumes; the velocities are computed in the centre of the faces and the cross components of the Reynolds tensor are attached to nodes located at the mid-edges. The biggest advantage of the staggered arrangement is the strong coupling between the velocities and pressure.

The pressure is treated by an implicit scheme, where a decoupling procedure for the pressure is derived from the Marker and Cell (MAC) algorithm proposed by Harlow and Welch [Harlow and Welch (1965)].

From the momentum conservation equation, a discrete Poisson equation is obtained for the pressure by enforcing mass conservation implicitly:

$$M * \bar{P}^{n+1} = B^n \tag{10}$$

The right hand side (B) of the linear system for the pressure is evaluated at the previous time step n, and the new pressure values are calculated at the next time step n+1. The matrix is symmetric and positive definite. Its coefficients only depend on the distance between grid nodes. The pressure is obtained by adopting either the Cholesky Factorization or the Preconditioned Conjugate Gradient (PCG). Note that the principle of mass flux continuity is imposed indirectly via the solution of Eq. 10. Convergence was declared when the maximum normalized sum of absolute residual $\tilde{\varepsilon}^n$ for each variable ϕ over all the computational domain was less than 10^{-4}. This maximum error is for each variable determined by:

$$\tilde{\varepsilon}^n = \max \sum_{i=1}^{N} (1 - \phi_i^n / \phi_i^{n+1}) \tag{11}$$

where N is the number of control volumes and being any flow variable.

It should be noted that the diffusion terms, in the momentum equation are treated using a second order accurate scheme in space. The convective terms are approximated by the quadratic upstream interpolation scheme (QUICK) [see Leonard (1979)]. Also, the mass conservation equation is evaluated at the time n+1, whereas the advection and diffusion terms in the moment equation are evaluated at the time n. To satisfy the CFL criteria, the time step Δt was restricted to a value satisfying

$$CFL_{\max} = \Delta t \max \left[\frac{|U|}{\Delta x} + \frac{|V|}{\Delta y} + \frac{|W|}{\Delta z} \right] \leq 0.3 \tag{12}$$

which corresponds to the choice $\Delta t = 0.054\nu/u_\tau^2$. For the present computation, the average value for the $CFL_{\max}$ is 0.22.

The advection terms in transport equations for k and ε are discretized in space using the first order upwind scheme.

4.2 Numerical details and boundary conditions

For the first time-step, at the inlet of the duct, a constant profile was given to $\overline{U}$, k and ε. The secondary velocities were initialised as nil (and) all over the domain. The k and ε inlet values were obtained from the DNS data using the r.s.m (root mean square) velocities and the eddy viscosity, that was about four times the molecular viscosity. At the outlet, a homogeneous Neumann boundary condition was used for the inlet condition. The same procedure is used for the following time-steps up to convergence.

The Reynolds number of 4410 is based on the bulk velocity and the hydraulic diameter of the duct. The calculations were carried out using 63×63 grid points, regularly spaced in the cross-section and 120 grid points in the streamwise direction. The outcome with this grid points was found to be satisfactory. The grid convergence was checked using 61×61 grid points in the cross-section, the maximum difference observed between the two calculations were less than 0.1% in the streamwise velocity near the corner. Mesh independence for the results has been checked with 100x21x21 and 90x41x41 finite volumes. For example, the maximum difference observed between the results from various mesh were less than 0.1% in the spanwise velocity near the wall.

The boundary condition values for k and ε, at the first grid point near the wall, was calculated taking into account the fact that this point was in the viscous sub-layer. Also, due to the use of a staggered grid, the value of and are not defined at the wall. In this paper, we consider the following boundary conditions for the equation of and , which have been used by Patel et al. [Patel, Rodi, and Scheuerer (1984)].

A condition for symmetry, homogeneous Neumann, was used for all the variables along the wall bisectors of the square duct.

4.3 Numerical results and discussion

Table 4 gives the summary of the various parameters of some studies considered in the literature. The Reynolds number Re_τ based on the shear velocity (u_τ) and the duct height ($H = 2h$) is defined as $Re_\tau = u_\tau H/\nu$, and the bulk Reynolds Re_b number based on the bulk streamwise velocity ($\overline{U}_b$) and the duct height is defined as $Re_b = \overline{U_b}H/\nu$. For reference, the following abbreviations are used in this table: SQD: Square duct; SQAD: Square annular duct; REQ: Rectangular duct.

4.3.1 Mean velocity field

The mean streamwise velocity along the wall-bisector is presented in Figure 9(c). Compared with DNS, experiments and other simulations, the mean streamwise from the Craft$_f$ et al.'s model is in good agreement with DNS and LES data, despite

Table 4: Studies considered in the literature.

Researcher	Channel type			Method
Gavrilakis (1992)	SQD	4410	300	DNS
Huser & Biringen (1993)	SQD	10320	600	DNS
Madabhushi & Vanka (1991)	SQD	5810	360	LES
Xu & Pollard (2001)	SQAD	3650	400	LES
Niederschulte (1989)	REQ	4914		Experiment
Gessner & Emery (1981)	REQ	250000		Experiment

the difference between the Reynolds numbers (see Tab. 4). However, experimental data causes a noticeable discrepancy in the region away from the wall. Figure 9(a and b) shows the streamwise mean velocity along the z direction at different sections, namely, at y/h=0.3 and y/h=0.7. In Figure 9(a and b), the simulated streamwise velocity is normalized by the mean centreline velocity U_0. It can be seen in Figure 9(a and b) that the mean streamwise velocity in the present RANS prediction agrees well with the results of Gavrilakis (1992).

The contours of mean streamwise velocity and secondary flow vectors in a quadrant of a cross-section are shown in the Figures 10 and 11, respectively. The mean streamwise velocity and secondary flow vectors from DNS data by Gavrilakis (1992) are also given for comparison. By the examination of Figure 10, we remark that the flow is symmetric according the corner bisector, and the prediction is in good agreement with DNS data.

The secondary velocities convect mean-flow momentum from the central region to the corner region along the corner bisectors. They also transport the low-momentum fluid to the center along the wall bisector. This results in the bulging of the streamwise-velocity contours towards the corner which can be seen in Figure 10. It can also be seen from this figure that a fair degree of symmetry over the quadrant has been obtained. It should be noted that the mean secondary velocity from the present RANS is less developed than those from DNS data by Gavrilakis (1992).

The contours of the z-component of the secondary velocity W/U_0 are shown in Figure 12. We can observe that the contours obtained by Craft et al.'s model are compared favourably with those of the DNS data of Gavrilakis.

In Figure 13(c), the secondary velocity component in z-direction along the wall bisector is compared with DNS of Gavrilakis (1992) and Huser and Biringen (1993), LES data of Xu and Pollard (2001) and experimental data of Gesssner and Emery (1981). Note that the Reynolds number of the flow in experiment by Gessner and Emery is much larger than of the simulated flow herein (see Tab. 4). The DNS re-

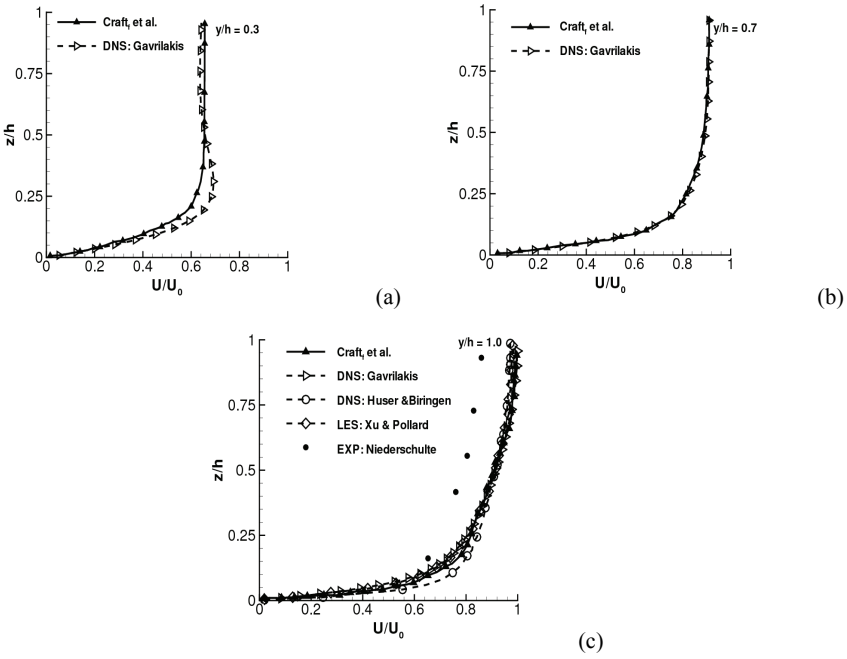

Figure 9: The normalized mean streamwise velocity U/U_0 at different sections $y/h = 0.3,\ 0.7\ and\ 1.0$.

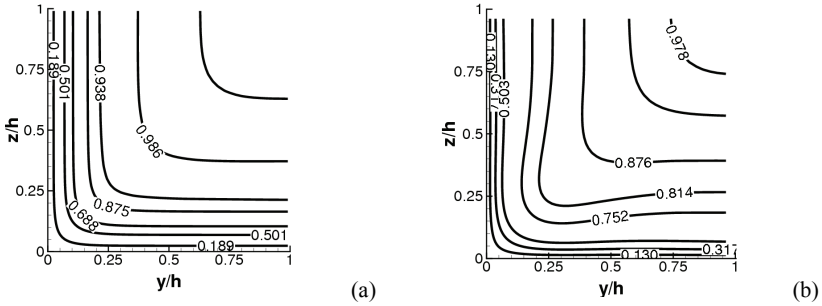

Figure 10: Contours of the normalized mean streamwise velocity U/U_0 in a quadrant: (a) present study; (b) DNS data from Gavrilakis (1992).

sults from both Gavrilakis (1992) and Huser and Biringen (1993), and the present RANS prediction are significantly lower than the experimental data, as seen in Fig-

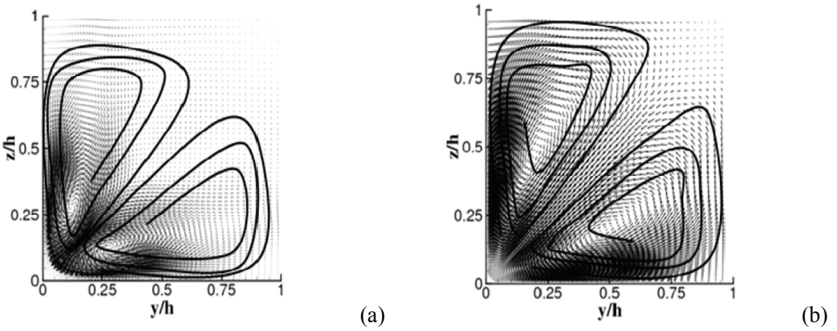

Figure 11: Mean secondary velocity vectors in a quadrant: (a) present study; (b) DNS data from Gavrilakis (1992).

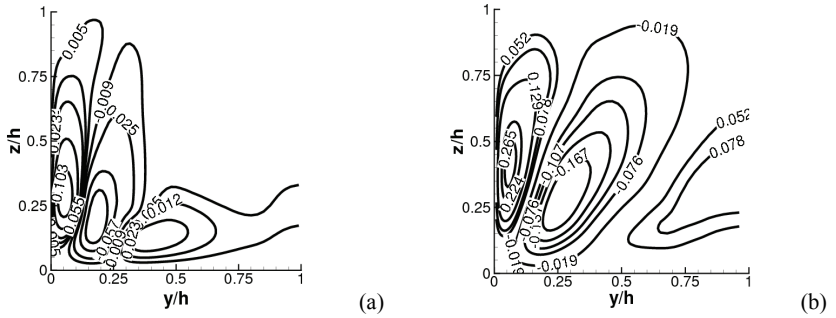

Figure 12: Contours of the normalized mean vertical velocity W/U_0 in a quadrant: (a) present study; (b) DNS data from Gavrilakis (1992).

ure 13(c), which is probably due to Reynolds number effects.

It can be seen in Figure 13(c) that the secondary velocity from the present RANS results agrees well with the DNS of Gavrilakis (1992) and Huser and Biringen (1993), especially in the region $z/h > 0.15$, and the LES from Xu and Pollard (2001) in the region $z/h > 0.45$. The distribution of the z-component of secondary velocity at different y/h locations, namely at $y/h = 0.3$ and $y/h = 0.7$, is shown in Figure 13(a and b). The present RANS results show good qualitative agreement with the DNS data of Gavrilakis (1992).

Contours of mean streamwise vorticity are shown in Figure 14. This quantity is a direct manifestation of the secondary flow. Again, there is very good qualitative agreement between the present RANS results and the DNS data of Gavrilakis

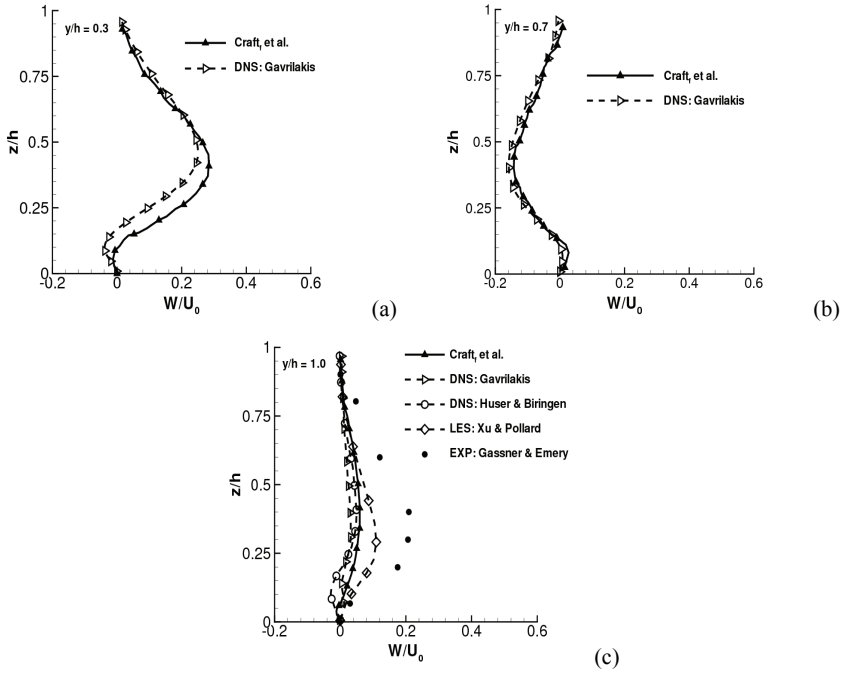

Figure 13: The normalized mean vertical velocity W/U_0 at different sections $y/h =$ 0.3, 0.7, 1.0.

(1992).

4.3.2 Turbulence statistics

The streamwise turbulence intensity along the wall bisector is presented in Figure 15. In this figure, DNS data by Gavrilakis [Gavrilakis (1992)] and Huser and Biringen [Huser and Biringen (1993)], LES data by Xu and Pollard [Xu and Pollard (2001)] and Madabhushi and Vanka [Madabhushi and Vanka (1991)], and experimental data by Niederschulte [Niederschulte (1989)], are provided for comparison with the present RANS data (Craft$_f$ et al.). The RANS results tend to slightly under-predict (about 7% compared with the DNS from Gravrilakis and 20% compared with the LES) in the near wall region. The peak value location from the current predictions and LES by Madabhushi and Vanka [Madabhushi and Vanka (1991)] is obtained at $z/h = 0.10$, whereas this location is at $z/h = 0.13$ in the DNS by Gavrilakis [Gavrilakis (1992)] and experimental data for Niederschulte [Niederschulte (1989)].

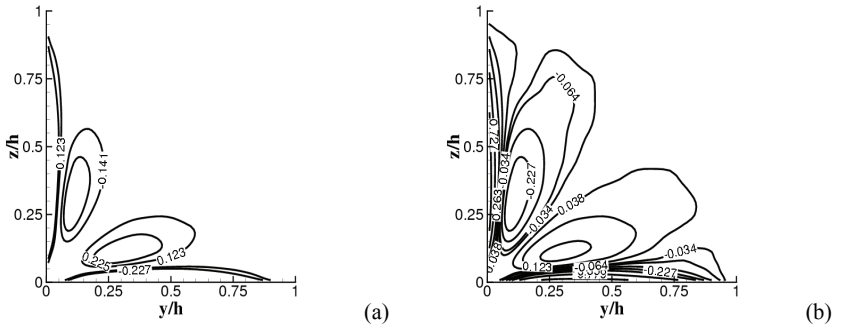

Figure 14: Distribution of the normalized mean streamwise vorticity: (a) present study; (b) DNS data from Gavrilakis (1992).

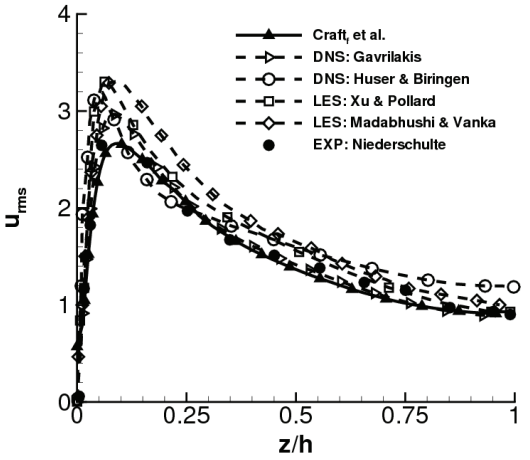

Figure 15: Streamwise turbulence intensity u_{rms} along the wall bisector ($y/h = 1.0$).

The DNS, LES and experimental were conducted at quite different Reynolds number (from 4410 to 10320). However, the agreement is satisfying and suggests that the near wall turbulence generation mechanisms are faithfully captured

The Figures 16 and 17 present, respectively, comparisons of the turbulence intensities, v_{rms} and w_{rms} in the wall normal z-direction. The present RANS results, while over-predicting the magnitude of v_{rms} by about 16% compared with the DNS from Gavrilakis (1992), 20% compared with the DNS from DNS from Huser and Biringen [Huser and Biringen (1993)], and about 30% compared with the LES results

and experimental data. It can be seen in Figure 16 that the turbulence intensity from the present RANS data agree with DNS data, LES data from Madabhushi and Vanka [Madabhushi and Vanka (1991)], and with measured data by Niederschulte (1989) for $z/h \leq 0.75$ and $z/h \geq 0.35$. In Figure 16, it is observed that the profiles of turbulence intensity w_{rms} well duplicate the DNS results. The profiles of turbulence intensity from LES data by Xu and Pollard [Xu and Pollard (2001)], and experimental data of Niederschulte (1989) appear to be smaller than the profile from the present RANS. Willmarth [Willmarth (1975)] and Balint et al. [Balint, Wallace, and Vukoslavcevic (1991)] suggested that the difference in the peak comes from the Reynolds number effect that all components of turbulence intensity increase with Reynolds number in the log region of wall-bounded turbulent flows. The difference in the other part of the profile also results from the same effect.

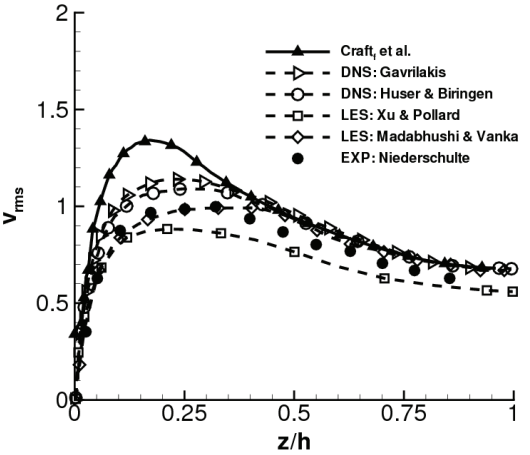

Figure 16: Cross-streamwise turbulence intensity v_{rms} along the wall bisector ($y/h = 1.0$).

Figure 18 shows the contour plots of the primary Reynolds stress $< uw >$. We can see clearly that the primary shear stress $- < uw >$ by the present RANS data shows a maximum value of 0.861 and a minimum value of -0.003, whereas the DNS data from Gavrilakis (1992) shows a maximum of 0.665 and a minimum of -0.166 in the same region of the quadrant.

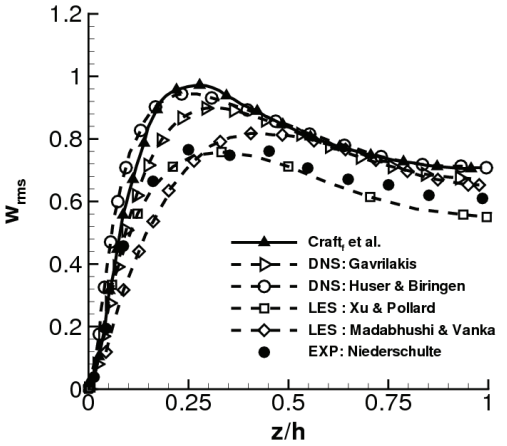

Figure 17: Cross-streamwise turbulence intensities w_{rms} along the wall bisector ($y/h = 1.0$).

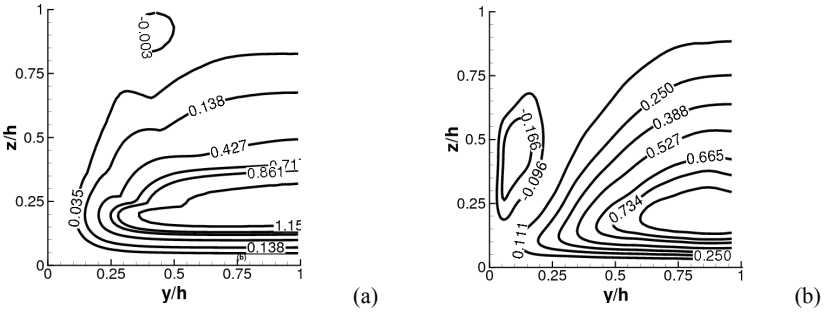

Figure 18: Primary Reynolds stresses $< uw >$: (a) present study; (b) DNS data from Gavrilakis (1992).

5 Conclusion

We have performed RANS simulation of the three-dimensional incompressible Navier-Stokes equations to study the turbulent flow within a duct of square cross-section. In order to carry out this work, we considered the explicit algebraic Reynolds stress model proposed by Craft et al. [Craft, Launder, and Suga (1996)].

Firstly, this EARSM model is studied using a priori procedure based on data resulting from the direct numerical simulation of Gavrilakis (1992).

We show that the Craft et al.'s model (1996) is realizable, since the analysis shows that the normal Reynolds stresses are always nonnegative and the Schwartz inequality is satisfied. The map of the second and third invariants for the Reynolds stress tensor indicates that within a quadrant the turbulence field comes close to one-, two-, and three-component states. To predict the significant viscous effects due to the presence of the wall and corner, damping functions are implemented. The comparison of the mean velocity field shows a good agreement. Overall, the Craft$_f$ et al. model considered in this work yields better predictions than those obtained by the original model.

Secondly, as its results are in a limited qualitative agreement with the DNS data, our RANS simulation is carried out using an a posteriori procedure. The simulation results were compared not only with Gavrilakis data but also with other numerical or experimental data sets. A good agreement with DNS (Gavrilakis, and Huser and Biringen), LES (Madabhushi and Vanka, and Xu and Pollard) and experimental (Niederschulte) results is achieved. The present RANS turns out to be able to correctly reproduce both the mean flow properties and turbulence statistics. Indeed, the profiles and maps of the mean velocity and turbulence statistics are in good agreement with the DNS, LES and experimental data in particular when one approaches the centre of the duct. Also, our RANS simulations, which are performed at a significantly reduced cost compared with DNS and LES, well reproduce the intensity of the secondary flow and the mean streamwise vorticity.

References

Ahrem, R.; Beckert, A.; Wendland, H. (2006): A meshless spatial coupling scheme for large-scale fluid-structure interaction problems. *CMES: Computers Modeling in Engineering and Sciences*, vol. 12, No. 2, pp. 121-136.

Aquelet, N.; Souli, M.; Gabrys, J.; Olovson, L. (2003): A new ALE formulation for sloshing analysis, *Int. J. of Structural Engineering and Mechanics*, vol. 16, pp. 423-440.

Arefmanesh, A.; Najafi, M.; Abdi, H. (2008): Meshless local Petrov-Galerkin method with unity test function for non-isothermal fluid flow. *CMES: Computers Modeling in Engineering and Sciences*, vol. 25, No. 1, pp. 9-22.

Balint, J.-L; Wallace, J. M.; Vukoslavcevic, P. (1991): The velocity and vorticity vector fields of turbulent boundary layer, Part 2: Statistical properties. *J. Fluid Mech.*, vol. 228, pp.53-86.

Craft, T. J.; Launder, B. E; Suga, K. (1996): Development and application of the cubic eddy-viscosity model of turbulence. *International J. Heat and Fluid flow*, vol. 17, 108-115.

Craft, T. J.; Lacovides, H.; Yoon, J. H. (1999): Progress in the use on non-linear two equation models in the computation of convective heat-transfer in impinging and separated flow. *Flow, Turbulence and Combustion*, vol. 63, pp. 59-80.

Gatski, T. B.; Rumsey, C. L. (2001): Linear and non-linear eddy-viscosity models. In: Launder B.E. and Sandham N.D. (Eds.), closure strategies for turbulent and transitional flows. *Cambridge University Press*, Cambridge, pp. 9–46.

Gatski, T. B.; Speziale, C. G. (1993): On explicit stress models for complex turbulent flows. *J. Fluid Mech.*, vol. 254, pp. 59-78.

Gavrilakis, S. (1992): Numerical simulation of low-Reynolds-number turbulent flow through a straight square duct. *J. Fluid Mech.*, vol. 224, pp. 101-129.

Gessner, F. B.; Emery, A. F. (1981): The numerical prediction of developing flow in rectangular ducts. *ASME Trans. J. Fluids Eng.*, vol. 103, pp. 445-455.

Gibson, M. M.; Launder, B. E. (1978): Ground effects on pressure fluctuations in the atmospheric boundary layer. *J. Fluid Mech.*, vol. 86, pp. 491-511.

Harlow, F. H.; Welch, J. E. (1965), Numerical calculation of time-dependent viscous incompressible flow or fluid with free surface. *Physics of Fluids*, vol. 8, pp. 2182-2189.

Huser, A.; Biringen, S. (1993): Direct numerical simulation for turbulent flow in a square duct. *J. Fluid Mech.*, vol. 257, pp. 65-95.

Jongen, T.; Mompean, G.; Gatski, T. B. (1998): Predicting S-duct flow using a composite algebraic stress model. *AIAA Journal*, vol. 36, pp. 327-335.

Launder, B. E.; Reece, G. J.; Rodi, W. (1975): Progress in the development of a Reynolds-stress turbulence closure. *J. Fluid Mech.*, vol. 68, pp. 537-566.

Launder, B. E.; Sharma, B. I. (1974): Application of the energy-dissipation model of turbulence to calculation of flow near a spinning disc. *Lett. Heat Mass Transfer*, vol. 1, pp. 131-138.

Leonard, B. P. (1979): A stable accurate convective modelling procedure based on quadratic upstream interpolation. *Computer Methods in Applied Mechanics and Engineering*, vol. 19, pp. 59-88.

Lin, H.; Atluri, S. N. (2001): The meshless local Petrov-Galerkin (MLPG) method for solving incompressible Navier-Stokes equations. *CMES: Computers Modeling in Engineering and Sciences*, vol. 2, No. 2, pp. 117-142.

Longatte, E.; Bendjeddou, Z.; Souli, M. (2003): Application of Arbitrary Lagrange Euler formulations to flow-induced vibration problems. *J. of Pressure Vessel and Technology*, Vol. 125, pp. 411-417.

Lumley, J. L.; Newman, G. (1977): The return to isotropy of homogeneous tur-

bulence. *J. Fluid Mech.*, vol. 82, pp. 161-178.

Madabhushi, R. K.; Vanka, S. P. (1991): Large-eddy simulation of turbulence-driven secondary flow in a square duct. *Phys. Fluids A*, vol. 3, no. 11, pp. 2734-2745.

Mompean, G.; Gavrilakis, S.; Machiels L.; Deville M. O. (1996): On predicting the turbulence-induced secondary flows using non-linear $k-\varepsilon$ models. *Phys. of Fluids*, vol.8, pp. 1856-1868.

Naji, H.; Mompean, G.; El Yahyaoui, O. (2004): Evaluation of explicit algebraic stress models using direct numerical simulations. *J. of Turbulence*, vol. 5:38-63.

Niederschulte, M. A. (1989): Turbulent flow through a rectangular channel, Ph.D. thesis, Univ. of Illinois at Urbana-Champaign, III.

Orsini, P.; Power, H.; Morvan, H. (2008): Improving volume element methods by meshless radial basis function techniques. *CMES: Computers Modeling in Engineering and Sciences*, vol. 23, No. 3, pp. 187-207.

Pasquim, B. M.; Mariani, V. C. (2008): Solutions for incompressible viscous flowin a triangular cavity using cartesian grid method. *CMES: Computers Modeling in Engineering and Sciences*, vol. 35, No. 2, pp. 113-132.

Patel, C.V.; Rodi, W.; Scheuerer, G. (1984): Turbulence models for near-wall and low Reynolds number flows: a review. *AIAA Journal*, vol. 23, pp. 1308-1319.

Pettersson, B. A.; Andersson, H. I. (2002): Prediction of Turbulence-generated secondary mean flow in square duct, Flow. *Turbulence and Combustion*, vol. 68, pp. 41-61.

Prandtl, L. (1952): The Essentials of Fluid Dynamics. *Blackie*, Glasgow.

Rodi, W. (1976): A new algebraic relation for calculating the Reynolds stresses. *ZAMM*, vol. 56, pp. 219-221.

Rubinstein, R.; Barton, J. M. (1990): Non-linear Reynolds models and the renormalisation group. *Phys. Fluids A*, vol.2, pp. 1472-1476.

Shih T. H.; Zhu J.; Lumley J. L. (1995): A new Reynolds stress algebraic equation model. *Comp. Appl. Mech. Eng.*, vol.125, pp. 287-302.

Shih, T. H.; Zhu, J.; Lumley, J. L. (1993): A realizable Reynolds stress algebraic equation model. NASA Tech. Memo., TM-105993.

Speziale, C. G. (1987): On non-linear $k-l$ and $k-\varepsilon$ models turbulence. *J. Fluid Mech.*, vol. 178, pp. 459-475.

Speziale, C. G.; Sarkar, S.; Gatski, T. B. (1991): Modelling the pressure-strain correlation of the turbulence: An invariant dynamical system approach. *J. Fluid Mech.*, vol. 227, pp. 245-272.

Speziale, C. G.; Younis, B. A.; Berger, S. A. (2000): Analysis and modelling of turbulence flow in an axially rotating pipe. *J. Fluid Mech.*, vol.407, pp. 1-26.

Taulbee, D. B. (1992): An improved algebraic Reynolds stress model and corresponding nonlinear stress model. *Phys. Fluids* A, vol.4, no. 11, pp. 2555-2561.

Van Driest, E. R. (1956): On turbulent flow near a wall. *J. Aeronautical Sciences*, vol. 23, pp. 1007-1011.

Vasquez, M. S.; Métais, O. (2002): Large eddy simulation of the turbulent flow through a heath square duct. *J. Fluid Mech.*, vol. 453, pp. 201-238.

Vertnik, R.; Šarler, B. (2009): Solution of incompressible turbulent flow by a mesh-free method. *CMES: Computers Modeling in Engineering and Sciences*, vol. 44, No. 1, pp. 65-95.

Wallin, S.; Johansson, A. V. (2000): An explicit algebraic Reynolds model for incompressible and compressible turbulent flows. *J. Fluid Mech.*, vol. 403, pp. 89-132.

Willmarth, W. W. (1975): Pressure fluctuations beneath turbulent boundary layers, *Ann. Rev. Fluid Mech.*, vol. 7, pp. 13-36.

Xu, H.; M. Khalid; Pollard, A. (2003): Large Eddy Simulation of turbulent flow in a confined square coaxial jet. *Inter. J. Comput. Fluid Dynamics*, vol. 17 (5), pp. 339-359.

Xu, H.; Pollard, A. (2001): Large eddy simulation of turbulence flow in square annular duct. *Physics of Fluids*, vol. 13, pp. 3321-3337.

Yap, C. R. (1987): Turbulent heat and momentum transfer in recirculating and impinging flows. Ph.D thesis, Faculty of Technology, University of Manchester, Manchester, UK.

Yoshizawa, A. (1984): Statistical analysis of the derivation of the Reynolds stress from its eddy-viscosity representation. *Physics of Fluids*, vol. 27, pp. 1377-1387.

Zheng, J.; Long, S.; Xiong, Y.; Li, G. (2009): A finite volume meshless local Petrov-Galerkin method for topology optimization design of the continuum structures. *CMES: Computers Modeling in Engineering and Sciences*, vol. 42, No. 1, pp. 19-34.